Diffusion of hydrogen within idealized grains of bcc Fe: A kinetic Monte Carlo study

Yaojun A. Du,[1] Jutta Rogal,[2,*] and Ralf Drautz[2]

[1]*Fakultät für Physik and Center for Nanointegration (CENIDE), Universität Duisburg-Essen, Lotharstraße 1, 47048 Duisburg, Germany*

[2]*Interdisciplinary Centre for Advanced Materials Simulation, Ruhr-Universität Bochum, 44780 Bochum, Germany*

(Received 11 June 2012; revised manuscript received 14 September 2012; published 14 November 2012)

Structural defects in materials such as vacancies, grain boundaries, and dislocations may trap hydrogen and a local accumulation of hydrogen at these defects can lead to the degradation of the materials properties. An important aspect in obtaining insight into hydrogen-induced embrittlement on the atomistic level is to understand the diffusion of hydrogen in these materials. In our study we employ kinetic Monte Carlo (kMC) simulations to investigate hydrogen diffusion in bcc iron within different microstructures. All input data to the kMC model, such as available sites, solution energies, and diffusion barriers, are obtained from first-principles calculations. We find that hydrogen mainly diffuses within the interface region with an overall diffusivity that is lower than in pure bcc Fe bulk. The concentration dependence of the diffusion coefficient is strongly nonlinear and the diffusion coefficient may even decrease with an increasing hydrogen concentration. To describe the macroscopic diffusion coefficient we derive an analytic expression as a function of hydrogen concentrations and temperatures which is in excellent agreement with our numerical results for idealized microstructures.

DOI: 10.1103/PhysRevB.86.174110 PACS number(s): 75.50.Bb, 81.40.Np, 61.72.Mm, 67.80.fh

I. INTRODUCTION

Hydrogen is a very common impurity in iron-based materials. It is incorporated into the material during production and service and exhibits a high mobility within the bulk phase. It has further been shown that microstructural defects in the material such as vacancies, dislocations, and grain boundaries can trap hydrogen impurities.[1–4] The resulting local accumulation of hydrogen at these defects can then lead to a degradation of the mechanical properties of the material, which is also referred to as hydrogen embrittlement.[5] To explain the complex mechanisms underlying hydrogen embrittlement various approaches have been developed including hydrogen-enhanced local plasticity (HELP),[6–8] hydrogen-enhanced decohesion (HEDE),[9–13] and superabundant vacancy formation.[14]

The most important aspects in trying to understand the behavior of hydrogen within a material and its role in hydrogen embrittlement are the hydrogen solubility, the interaction of hydrogen with defects, and the hydrogen mobility. The solubility of hydrogen within pure bcc Fe is relatively low. Point and extended defects, however, can provide interstitial sites that are energetically much more favorable for hydrogen than the tetrahedral site in bcc Fe. In a recent study we investigated the solution energy of H in the presence of open and close-packed grain boundaries (GB) in bcc and fcc Fe[15] employing density-functional theory (DFT)[16,17] calculations. We find that in general hydrogen prefers the interstitial sites within the grain boundary region (with the exception of close-packed grain boundaries in fcc Fe). In particular we find a large energy gain of 0.4–0.5 eV for hydrogen interstitials at the $\Sigma5[001](310)$ grain boundary in bcc Fe ($\Sigma5$ in short) as compared to the bulk region. This indicates that hydrogen segregates to the grain boundary and is trapped there.

The mobility of hydrogen within pure bcc Fe bulk is high. The calculated diffusion barrier for H atoms moving between neighboring tetrahedral sites is $\sim$0.1 eV.[15,18] This is consistent with earlier experimental observations indicating that H diffuses rapidly within bcc metals.[19–23] Experimental studies investigating the diffusion of hydrogen in the presence of dislocations, grain boundaries, and phase boundaries show that the measured diffusivity depends on the hydrogen concentration.[24] In bulk Pd, Pd grain boundaries, and Pd/Al_2O_3 phase boundaries, the diffusion constant generally increases with increasing H concentration.[24] Within a theoretical study employing kinetic Monte Carlo (kMC) simulations it was illustrated that the attraction of H to screw dislocations in Fe materials can significantly affect H diffusion.[2] To properly evaluate the mobility of hydrogen within a certain material it is thus important to also consider the effect of the microstructure.

In this study, we employ kMC simulations to address H diffusion in the presence of grain boundaries in bcc Fe. In a previous study we found that the H diffusion barriers within the grain boundary region of bcc Fe are much higher (0.25–0.6 eV)[15] than in the bulk region. This suggests that H interstitials diffuse relatively slowly or are effectively immobile within the grain boundary interface, and that therefore the grain boundaries do not provide fast diffusion channels for hydrogen. Utilizing the information about available interstitial sites, diffusion barriers, and solution energies extracted from our DFT calculations, we set up a series of kMC models that represent idealized microstructures. The first model is an idealized cubic grain structure in bcc Fe, with and without point defects included in the bulk region of the grain. Since the model grains are much smaller than grains in the actual material we consider in our second model a parallel arrangement of grain boundary interfaces. This layered structure naturally introduces an anisotropy in the diffusivity. The third model presented in this paper represents a more detailed structure of the $\Sigma5$ grain boundary in bcc Fe. Within the above models, H diffusion constants are determined as a function of H concentrations and temperatures. From the results obtained within these model systems general trends for H diffusivity in various structural environments can be extracted. We then compare the numerical results to the derived analytic expression that describes the macroscopic diffusivity of hydrogen in different microstructures.

The paper is organized as follows. The computational approach is detailed in Sec. II. In Secs. III and IV the results for H diffusion within the idealized cubic grain structure with and without additional point defects are presented. The results for the layered structure and for the more detailed model of the Σ5 grain boundary are discussed in Secs. V and VI, respectively. Our findings are summarized in Sec. VII.

II. COMPUTATIONAL APPROACH

A. Kinetic Monte Carlo

We employ kinetic Monte Carlo[25,26] simulations to investigate H diffusion under various conditions and within a number of idealized microstructures. Within kMC simulations the time evolution of the system is described by a stochastic trajectory. The system states along this trajectory are connected by processes associated with certain probabilities. Here, we use a lattice approach; i.e., possible atomic positions are mapped onto a lattice and the system can evolve by atoms (hydrogen) hopping between neighboring lattice sites (interstitial sites in bcc Fe bulk and grain boundaries). Within harmonic transition state theory[27] the microscopic rate constant for a hop, k_i, associated with process i can be written as

$$k_i = \nu_{0,i} \exp(-\Delta E_i / k_B T), \tag{1}$$

where $\nu_{0,i}$ is the attempt frequency, k_B is the Boltzmann constant, T is the temperature, and ΔE_i is the energy barrier associated with process i. For all processes that can occur within our kMC models the corresponding energy barriers were calculated employing DFT calculations. Transition states were identified using the nudged elastic band method[28,29] as implemented in the VASP code.[30,31] In all calculations the generalized gradient approximation (GGA, PW91)[32,33] was used for the exchange-correlation functional. Convergence with respect to the energy cutoff for the plane waves and the integration of the Brillouin zone was ensured (details regarding the DFT calculations can be found in Ref. 15). For a given system configuration the sum over all rate constants of all possible processes is evaluated, $k_{tot} = \sum_i k_i$, and a process p to move to the next system state is chosen according to

$$\sum_{i=0}^{p-1} k_i < \rho_1 k_{tot} \leqslant \sum_{i=0}^{p} k_i, \tag{2}$$

where ρ_1 is a uniform random number between 0 and 1. Since the kMC algorithm simulates a sequence of Poisson processes, the real time evolution for each kMC step can be evaluated as[34]

$$t \rightarrow t - \ln(\rho_2)/k_{tot}, \tag{3}$$

where ρ_2 is a second random number between 0 and 1.

The diffusion constant tensor is calculated from the mean square displacement of the hydrogen atoms. To obtain better statistics on the diffusion constants we follow an approach outlined previously[2,24,35] and divide the kMC trajectory into a number of segments. The diffusion constant is calculated as the time-weighted average of the diffusion constants for each segment i,

$$D_{kk} = \sum_i D_{kk,i} \Delta t_i / t, \tag{4}$$

where for the tetragonal structures analyzed in this paper the diagonal components of the diffusion tensor D_{kk} suffice; $\Delta t_i = t_i - t_{i-1}$ is the time length of segment i, t is the total length of the kMC trajectory, and

$$D_{kk,i} = \langle [r_k(t_i) - r_k(t_{i-1})]^2 \rangle / 2\Delta t_i \tag{5}$$

is the diffusion constant for segment i. Here, $r_k(t_i)$ is the position of a H atom in the k direction (with $k = x,y,z$) at time t_i and $\langle \cdots \rangle$ denotes the average over all particles. The overall diffusion constant D is is defined as the average of the diagonal components of the diffusion tensor, $D = \frac{1}{3} \sum_k D_{kk}$.

Similarly, we define the probability p_s of finding hydrogen atoms in certain sites s (e.g., bulk, interface, or point defect sites) as

$$p_s = \frac{\sum_i p_{i,s} \Delta t_i}{t}, \tag{6}$$

with

$$p_{i,s} = \frac{N_{i,\mathrm{H},s}}{N_\mathrm{H}}, \tag{7}$$

where N_H is the total number of hydrogen atoms in the simulation and $N_{i,\mathrm{H},s}$ is the number of hydrogen atoms at site type s in the trajectory segment i.

B. Analytic description of the diffusion constant

The analytic expression for the diffusion constant D within a symmetric lattice and in the limit of low hydrogen concentrations is given by the classical Arrhenius expression

$$D = D_0 \exp(-\Delta E / k_B T), \tag{8}$$

with $D_0 = \Gamma a_0^2 \nu_0$. ΔE is the diffusion barrier, a_0 is the jump distance for a diffusion hop, and Γ is a geometric prefactor that is related to the connectivity of each site to its neighboring sites. For isotropic diffusion the geometric prefactor follows[36]

$$\Gamma = \frac{n}{2d}, \tag{9}$$

where n is the number of equivalent nearest neighbor sites and d is the dimensionality of the system.

To obtain an analytic expression for the probability to find hydrogen in various types of interstitial sites we assume a grand canonical ensemble and express the total number of H atoms within the system as[24]

$$N_\mathrm{H} = \sum_s \frac{n_s}{1 + \exp[(E_s - \mu)/k_B T]}, \tag{10}$$

where the sum runs over the various interstitial site types s, n_s is the number of sites of type s, E_s is the solution energy of hydrogen at site type s, and μ is the chemical potential. The probability to find hydrogen at site type s is therefore

$$p_s = \frac{N_{\mathrm{H},s}}{N_\mathrm{H}} = \frac{1}{N_\mathrm{H}} \frac{n_s}{1 + \exp((E_s - \mu)/k_B T)}. \tag{11}$$

The analytic results for the probability of finding hydrogen in certain sites can directly be compared with our numerical results employing Eq. (6).

C. H-H interactions

The analytic expression is strictly only valid for an idealized model system without any interactions between hydrogen atoms. However, in bcc Fe hydrogen atoms show repulsive nearest-neighbor interactions, which influences solution energies as well as diffusion barriers. To fully include these interactions requires a more sophisticated treatment of the Fe-H system. To account for the effect of H-H interaction to a first approximation we express the total energy of a configuration including pair interactions

$$E^{\text{tot}} = \sum_i E_i + \sum_{i,j>i} V_{ij}^{\text{pair}}. \tag{12}$$

Here, E_i is the solution energy of a H atom at a particular site for the noninteracting case and V_{ij}^{pair} is the pair interaction. The pair interactions are extracted from DFT calculations[37] using[8]

$$\begin{aligned} V^{\text{pair}} = {} & E^{\text{tot}}(\text{Fe}_{128}\text{H}_2) - E^{\text{tot}}(\text{Fe}_{128}) \\ & - 2[E^{\text{tot}}(\text{Fe}_{128}\text{H}) - E^{\text{tot}}(\text{Fe}_{128})], \end{aligned} \tag{13}$$

where $E^{\text{tot}}(\text{Fe}_{128})$ is the total energy of a 128 atom bcc Fe supercell, and $E^{\text{tot}}(\text{Fe}_{128}\text{H})$ and $E^{\text{tot}}(\text{Fe}_{128}\text{H}_2)$ are the total energies of the same cell containing one and two additional H atoms, respectively. Within the DFT calculations a configuration with H atoms in first-nearest-neighbor sites is not stable and thus occupation of nearest-neighbor sites is excluded within the kMC model. For H atoms in second- and third-nearest-neighbor sites we obtain $V_2^{\text{pair}} = 0.131$ eV and $V_3^{\text{pair}} = 0.059$ eV. The influence of the H-H interaction on the diffusion barriers, ΔE, is then approximated by[38]

$$\Delta E = \begin{cases} \Delta E_{\text{min}} & \text{if} \quad \frac{1}{2}\Delta E^{\text{tot}} < -\Delta E_0, \\ \Delta E_{\text{min}} + \Delta E^{\text{tot}} & \text{if} \quad \frac{1}{2}\Delta E^{\text{tot}} > \Delta E_0, \\ \Delta E_0 + \frac{1}{2}\Delta E^{\text{tot}} & \text{otherwise.} \end{cases} \tag{14}$$

Here, $\Delta E^{\text{tot}} = E_{\text{FS}}^{\text{tot}} - E_{\text{IS}}^{\text{tot}}$ is the difference in total energy between the initial (IS) and final (FS) state of a kMC move as obtained from Eq. (12). ΔE_{min} is the minimum barrier that must be overcome even for large energy differences between initial and final states and is set to 0.088 eV. The values of ΔE_0 are given by the diffusion barriers when H interactions are neglected (see Table I).

Based on hydrogen diffusion in perfect bcc Fe, the zero-point energy (ZPE) correction to the H diffusion barriers is estimated to be less than 50 meV.[18] This value is much smaller than the differences between the respective diffusion barriers in the bulk and the interface and in between the bulk and interface regions (see Table I). It is thus not expected that the ZPE corrections will significantly influence the obtained results and are thus not explicitly considered in the current study.

TABLE I. Diffusion barriers between various sites i within the idealized cubic grain. ΔE_i denote the barriers for a single H atom, $\Delta E_{0,i}$ are the corresponding values entering Eq. (14) including H-H interaction. All values are given in eV.

Process i	ΔE_i (eV)	$\Delta E_{0,i}$
bulk site → bulk site	0.088	0.088
bulk site → interface site	0.088	0.344
interface site → bulk site	0.600	0.344
interface site → interface site	0.250	0.250
bulk site → point defect	0.088	0.419
point defect → bulk site	0.750	0.419

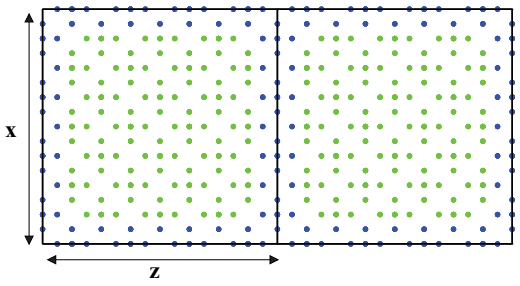

FIG. 1. (Color online) Model of an idealized cubic grain in bcc Fe. The spheres represent tetrahedral interstitial sites in bcc Fe, each having four nearest neighbors at the same distance. Interface sites are shown in blue, and bulk sites are shown in green.

III. IDEALIZED CUBIC GRAIN

To study hydrogen diffusion within an idealized cubic grain structure of bcc Fe we use the model shown in Fig. 1. In this simple model we only consider two different site types, bulk and interfaces sites, shown as blue and green spheres in Fig. 1, respectively. All sites in the kMC model are arranged as tetrahedral sites in bcc Fe (preferred interstitial site for hydrogen), each having four nearest neighbors at the same distance. Thus the two site types have the same geometry, but different solution energies and respective diffusion barriers. The grain boundaries between bulk regions are represented by three layers of interface sites. Within the kMC simulations we use a simulation cell with a side length of $x = 45.312$ Å containing 5952 interface and 43 200 bulk sites. The simulation cell is periodically repeated in all three dimensions.

The total number of H atoms within the system is

$$N_{\text{H}} = N_{\text{H,intf}} + N_{\text{H,bulk}}, \tag{15}$$

where $N_{\text{H,intf}}$ and $N_{\text{H,bulk}}$ are the number of H atoms at the interface and bulk sites, respectively. When the H-H interactions are neglected, we can correspondingly express the number of H atoms within the two site types as

$$N_{\text{H,intf}} = \frac{n_{\text{intf}}}{1 + \exp[(E_{\text{intf}} - \mu)/k_B T]} \tag{16}$$

and

$$N_{\text{H,bulk}} = \frac{n_{\text{bulk}}}{1 + \exp[(E_{\text{bulk}} - \mu)/k_B T]}. \tag{17}$$

The probability of finding H at bulk sites is therefore

$$p_{\text{bulk}} = \frac{N_{\text{H,bulk}}}{N_{\text{H,bulk}} + N_{\text{H,intf}}}. \tag{18}$$

To determine the solution energies and respective diffusion barriers between the two site types we use the results of our recent DFT study.[15] The bulk sites in our model correspond to tetrahedral interstitial sites in bcc Fe, and the interface sites correspond to the most stable interstitial site within the grain boundary region of the Σ5 GB. According to our DFT calculations the interstitial site at the Σ5 GB provides

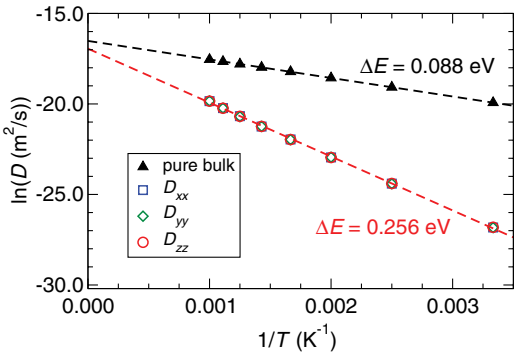

FIG. 2. (Color online) Logarithm of the diffusion constants for hydrogen as a function of the inverse temperature within the dilute limit. The black triangles are the results for hydrogen diffusion between tetrahedral sites in perfect bcc Fe. The blue, green, and red symbols represent the diagonal components of the diffusion tensor for the idealized cubic grain structure confirming an isotropic diffusion of hydrogen. The dashed lines correspond to linear fits of the kMC data.

a trap for H interstitials with a binding energy of $\Delta E_{\text{bind}} = E_{\text{bulk}} - E_{\text{intf}} = 0.512$ eV. There are four different processes for hydrogen diffusion between bulk and interface sites: bulk $\rightarrow$ bulk, bulk $\rightarrow$ interface, interface $\rightarrow$ bulk, and interface $\rightarrow$ interface. The energy barriers, ΔE_i, to determine the rate constants for these processes according to Eq. (1) are likewise taken from our recent DFT study[15] and are listed in Table I. The attempt frequency ν_0 is set to 10^{13} s^{-1} for all processes.

In Fig. 2 results for hydrogen diffusion constants for the cubic grain structure and for a perfect bulk structure are compared within the dilute limit. The perfect bulk structure contains only bulk sites with a diffusion barrier of 0.088 eV between neighboring sites and serves as a reference within our simulations. In Fig. 2 the logarithm of the diffusion constants is shown as a function of the inverse temperature. If we assume an Arrhenius-like behavior, see Eq. (8), then the slope corresponds to $-\Delta E/k_{\text{B}}$ and the y intercept corresponds to $\ln(D_0)$. For our reference, the perfect bulk system, a barrier of $\Delta E = 0.088$ eV is extracted from the slope. We obtain $\ln(D_0) = -16.52$, as expected from the theoretical value of $\ln(\Gamma a_0^2 \nu_0)$ with $\Gamma = 4/6$, $a_0 = 1.001$ Å, and $\nu_0 = 10^{13}$. Within the grain structure the three diagonal components of the diffusion tensor, D_{xx}, D_{yy}, and D_{zz}, are equivalent confirming the isotropic diffusion of hydrogen. The slope of the linear fit to the simulation data yields a value for the effective diffusion barrier of $\Delta E = 0.256$ eV, which corresponds to the barrier for an interface $\rightarrow$ interface hop, suggesting that diffusion mainly takes place within the interface region. The fitted value of $\ln(D_0) = -16.95$ is smaller than in perfect bulk. Assuming that the diffusion only takes place within the interface region and each interface site has only two adjacent interface sites, i.e., $\Gamma = 2/6$, one can obtain a theoretical value of $\ln(D_0) = -17.21$. It can also be seen that within the dilute limit diffusion is slower in the grain structure than in the perfect bulk structure. This can be explained by the fact that within the grain structure hydrogen is confined to the interface region which exhibits a higher barrier for diffusion.

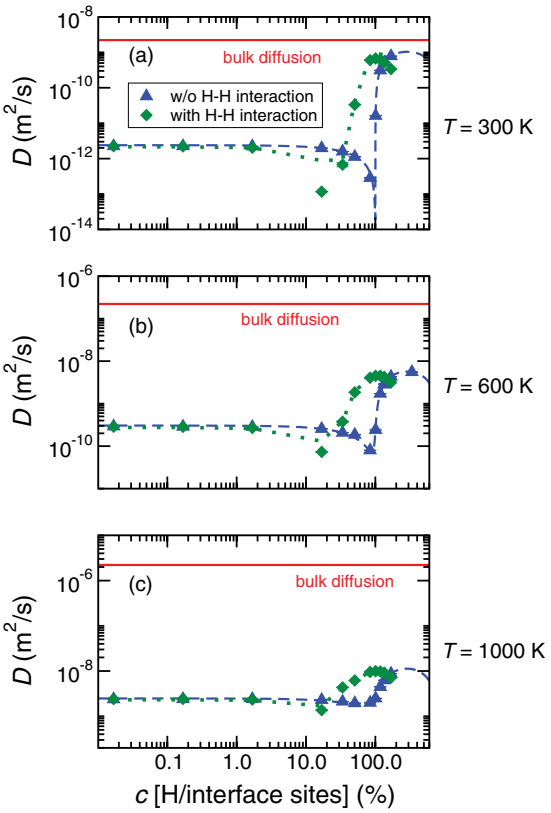

FIG. 3. (Color online) Diffusion constants as a function of H concentrations in an idealized cubic grain for temperatures of (a) 300 K, (b) 600 K, and (c) 1000 K. The blue triangles denote numerical results from the kMC simulations without H-H interactions; the dashed lines are obtained from Eq. (19). The green diamonds are obtained from kMC simulations with H-H interactions; the dotted line marks the analytic results (see Appendix). The red curve represents the diffusivity of H in perfect bcc Fe within the dilute limit.

In Fig. 3 hydrogen diffusion constants as a function of H concentration are shown for temperatures of $T = 300$, 600, and 1000 K. The kMC results without H-H interaction are illustrated by blue triangles; the results including H-H pair interactions are shown as green diamonds. In the case without H-H interactions the diffusivity is constant for low H concentrations for all three temperatures, it then decreases as the number of H atoms approaches the number of interface sites, before it again increases quickly to a considerably higher value. This behavior can be explained as follows: (I) At low H concentrations diffusion mainly takes place in the interface region and the associated diffusivity is lower than in perfect bulk (red line in Fig. 3) due to a higher diffusion barrier in the interface region; (II) when the H concentration approaches the number of interface sites, a dip occurs in the diffusion constant. This is due to blocking in the interface region; i.e., hydrogen is mainly confined to the interface region filling all the interface sites and effectively blocking diffusion processes. (III) At high H concentrations ($N_{\text{H}} > n_{\text{intf}}$), the overall diffusivity results mainly from bulk diffusion, which is much faster and thus the diffusivity increases. The dip in the diffusivity for hydrogen concentrations close to the number of interface sites is less pronounced for higher temperatures, because at higher

temperatures H atoms have a higher probability of escaping from the interface to the bulk region. At very high hydrogen concentrations the diffusivity decreases again due to blocking in the bulk region.

Our numerical results from the kMC simulations can also be described by an analytic expression. The overall diffusion constant is a combination of diffusion in the interface and in the bulk region and can thus be approximated as the weighted sum over the two contributions:

$$D(T,N_{\mathrm{H}}) = \sum_s p_s(T) D_{0,s} \exp\left(\frac{-\Delta E_s}{k_{\mathrm{B}}T}\right) \Xi_s(T,N_{\mathrm{H}}). \quad (19)$$

The sum is weighted by the probabilities p_s of being in the bulk or interface region; see Eq. (11). In addition the blocking[39] in the two regions is accounted for by the factor

$$\Xi_s(T,N_{\mathrm{H}}) = \left(1 - \frac{\overline{N}_{\mathrm{H},s}(T,N_{\mathrm{H}})}{n_s}\right), \quad (20)$$

where $\overline{N}_s(T,N_{\mathrm{H}}) = p_s(T)N_{\mathrm{H}}$ is the average number of hydrogen atoms at site type s and n_s is the number of sites of type s. Diffusion in between the two site types is assumed to be in equilibrium and these processes do not significantly contribute to the overall diffusivity. The prefactor $D_{0,s}$ contains the geometric prefactor Γ_s, the attempt frequency ν_0, and the hopping distance a_0, with $\nu_0 = 10^{13}$ s^{-1} and $a_0 = 1.001$ Å. The geometric prefactors for the bulk and interface regions, Γ_{bulk} and Γ_{intf}, are obtained by fitting to the numerical kMC data.

Before comparing the analytic and numerical results of the diffusion constants we verify that the hydrogen concentration in the two regions is indeed in equilibrium. For this, we evaluate the probability to be in the bulk region, p_{bulk}, within our kMC simulation according to Eq. (6) and compare it to the analytic result in Eq. (11). In Fig. 4 the results are shown for a temperature of $T = 600$ K. The analytic result agrees well with the kMC results. For high H concentrations, p_{bulk} converges to the theoretical limit $n_{\mathrm{bulk}}/(n_{\mathrm{bulk}} + n_{\mathrm{intf}})$. Comparing Figs. 3 and 4, one can find that for a wide range of concentrations, hydrogen is indeed confined to the interface region, even at $T = 600$ K. Only when the interface sites are filled with hydrogen, diffusion in the bulk region enhances the overall diffusivity.

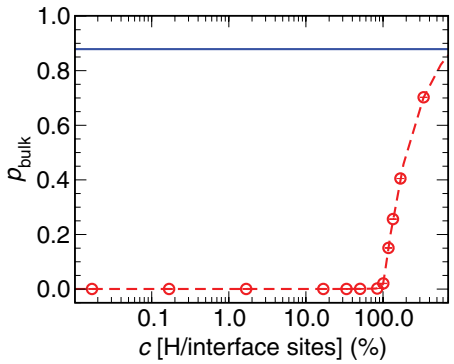

FIG. 4. (Color online) Probability of finding hydrogen in the bulk region of an idealized cubic grain at $T = 600$ K as a function of H concentration. The circles represent numerical results from the kMC simulations; the dashed line shows the result from the grand canonical ensemble model [see Eq. (11)]. The solid blue line marks the theoretical limit $n_{\mathrm{bulk}}/(n_{\mathrm{bulk}} + n_{\mathrm{intf}})$.

Using our kMC data at $T = 300$, 600, and 1000 K, the geometric prefactors are $\Gamma_{\mathrm{intf}} = 0.377$ and $\Gamma_{\mathrm{bulk}} = 0.644$. As shown in Fig. 3, the analytic results are in excellent agreement with the kMC results. The fitted values for the geometric prefactors also agree well with their theoretical values. In the bulk region each site has four nearest neighbors yielding $\Gamma_{\mathrm{bulk}} = 4/6 = 0.667$, whereas the interface region is a 3D network of 2D grain boundary plains with only two nearest neighbors for each interface site, yielding $\Gamma_{\mathrm{intf}} = 2/6 = 0.333$. The small deviation of the numerical fitted values from the ideal theoretical ones is mainly due to diffusion processes in the vicinity of neighboring bulk and interface sites where the local connectivity differs from the ideal one.

Including H-H interactions in our kMC model we observe a change in the diffusivity compared to neglecting H-H interactions as the H concentration approaches the number of available interface sites. But the overall shape of the curves remains the same: a constant diffusivity at low H concentrations, then a dip that becomes shallower with increasing temperature, and finally a strong increase due to contributions from bulk diffusivity is observed. The dip, however, occurs at a lower H concentration. This results from effective increase in blocking due to the strongly repulsive nearest-neighbor interactions. To describe the diffusivity including the H-H interaction with a simple analytic formula is not possible. Since the solution energies as well as diffusion barriers depend on the H-H interactions, also the probability of finding H at a certain site type as well as the blocking factor are no longer simple functions of the number of H atoms. Thus Eqs. (11) and (19) cannot be applied. We used the numerical probabilities from our kMC simulations and a modified blocking factor to estimate the applicability of our analytical approach (details are given in the Appendix). The results are shown as dotted green lines in Fig. 3. The numerical and analytical results compare reasonably well, but especially the depth of the dip for lower temperatures is not well reproduced. This suggests that the more complex interplay of diffusion processes resulting from simple H-H pair interactions could not easily be reproduced by a simple mean-field approach.

IV. IDEALIZED CUBIC GRAIN WITH ISOLATED POINT DEFECTS

In addition to the interface and bulk sites we next included point defects in the bulk region as a third site type into our model. Point defects such as vacancies or substitutional atoms are typically present in materials and may as well influence the diffusion of hydrogen. Within our idealized cubic grain model we include 400 and 40 point defect sites corresponding to a point defect concentration of about 0.80% and 0.08%, respectively. The point defect sites have the same geometry as bulk and interface sites, but different energetics. Since hydrogen binds even stronger to vacancies than to interface sites,[40] the point defect sites are also considered to be more stable in our kMC model. The corresponding microscopic diffusion barriers are summarized in Table I.

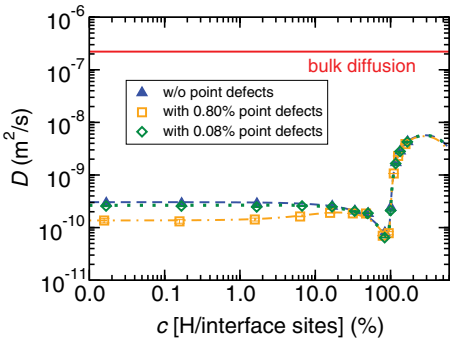

FIG. 5. (Color online) Diffusion constants as a function of H concentration at $T = 600$ K in an idealized cubic grain [blue (dark) triangles] and in an idealized grain with an additional 0.80% [orange (light) squares] and 0.08% (green diamonds) point defects in the bulk region. The symbols denote results from the kMC simulations; dashed/dotted lines indicate analytic results according to Eq. (19). The red curve represents the diffusivity of H in perfect bcc Fe within the dilute limit.

Since the point defects are not connected to each other there is no direct hop from one point defect to the next. Hence, the geometric prefactor Γ_{trap} for point defects in Eq. (19) is expected to be zero. However, the point defects alter the distribution of hydrogen within the system and thus the corresponding probabilities p_s.

In Fig. 5 the results for H diffusivities in an idealized cubic grain with and without point defects are compared for a temperature of $T = 600$ K. For a high defect concentration and at low H concentrations most hydrogen atoms are trapped at the point defects and hence do not directly contribute to the overall diffusivity. Therefore, the diffusion constants are lower as compared to those in the same grain without point defects. At higher H concentrations the effect becomes less pronounced and eventually all point defects and interface sites are filled, and hydrogen atoms in the bulk region dominate the overall diffusion. At lower defect concentrations the effect becomes almost negligible.

For the grain model including point defects the fitted geometric prefactors for the interface region, bulk region, and point defects are $\Gamma_{\text{intf}} = 0.376/0.369$, $\Gamma_{\text{bulk}} = 0.634/0.640$, and $\Gamma_{\text{trap}} = 0.0/0.0$ for high/low defect concentrations, respectively. The analytical results obtained from Eq. (19) are in excellent agreement with the kMC results as shown in Fig. 5. Note that the fitted geometric prefactors for the model without point defects are $\Gamma_{\text{intf}} = 0.377$ and $\Gamma_{\text{bulk}} = 0.644$. The geometric prefactor for the bulk region decreases slightly in the presence of point defects, since the point defects reduce the effective number of equivalent nearest-neighbor sites within the bulk region.

The defect concentrations assumed here are very high as compared to the vacancy concentration in pure Fe. The formation energy of a vacancy in bcc Fe, E_f, is around 1.7 eV.[41] The average number of point defects, N_p, at a temperature T is given by

$$N_p = n_i \exp\left(\frac{-E_f}{k_B T}\right). \tag{21}$$

Our kMC model represents $n_i \approx 4000$ Fe sites, which yields $N_p = 1.3 \times 10^{-11}$. Thus, at realistic defect concentrations the diffusivity within the interface region will hardly be effected.

In the limit of low hydrogen concentrations and low temperatures Eq. (19) reduces to an expression previously used to describe H diffusion in the presence of point traps in iron materials.[2,42] Assuming there are only bulk and isolated point defect trapping sites with $\Gamma_{\text{trap}} = 0.0$, Eq. (19) reads

$$D(T, N_{\text{H}}) = p_{\text{bulk}} D_{0,\text{bulk}} \exp\left(\frac{-\Delta E_{\text{bulk}}}{k_B T}\right) \Xi_{\text{bulk}}(T, N_{\text{H}}), \tag{22}$$

with

$$p_{\text{bulk}} = \frac{\frac{n_{\text{bulk}}}{1+\exp[(E_{\text{bulk}}-\mu)/k_B T]}}{\frac{n_{\text{trap}}}{1+\exp[(E_{\text{trap}}-\mu)/k_B T]} + \frac{n_{\text{bulk}}}{1+\exp[(E_{\text{bulk}}-\mu)/k_B T]}}. \tag{23}$$

For both low H concentrations and low temperatures we can approximate $\exp(E_i - \mu/k_B T) \gg 1$ and

$$\begin{aligned} p_{\text{bulk}} &\approx \frac{\frac{n_{\text{bulk}}}{\exp[(E_{\text{bulk}}-\mu)/k_B T]}}{\frac{n_{\text{trap}}}{\exp[(E_{\text{trap}}-\mu)/k_B T]} + \frac{n_{\text{bulk}}}{\exp[(E_{\text{bulk}}-\mu)/k_B T]}} \\ &= \frac{1}{1 + \frac{n_{\text{trap}}}{n_{\text{bulk}}} \exp\left(\frac{\Delta E_{\text{bind}}}{k_B T}\right)}, \end{aligned} \tag{24}$$

where $\Delta E_{\text{bind}} = E_{\text{bulk}} - E_{\text{trap}}$ is the binding energy of hydrogen to the trapping site. Furthermore, for low H concentrations $\Xi_{\text{bulk}} \to 1$ and substituting Eq. (24) into Eq. (22) leads to the known expression[2,42]

$$\begin{aligned} D(T) = D_{0,\text{bulk}} &\exp\left(\frac{-\Delta E_{\text{bulk}}}{k_B T}\right) \\ &\times \left[1 + \exp\left(\frac{\Delta E_{\text{bind}}}{k_B T}\right) \frac{n_{\text{trap}}}{n_{\text{bulk}}}\right]^{-1}. \end{aligned} \tag{25}$$

As can be seen from Eq. (25) the effect of point defects becomes negligible for small numbers of trapping sites, a small binding energy, or high temperatures.

V. IDEALIZED LAYERED STRUCTURE

The idealized cubic grains discussed in Secs. III and IV are small compared to typical grain sizes in materials. In atomistic simulations grain boundary structures are thus often modeled as parallel arrangements of interface planes to describe their 2-dimensional nature. As a second microstructure model we investigate the diffusion of hydrogen within such an idealized layered structure as shown in Fig. 6.

All sites in the kMC model reflect the geometry of tetrahedral interstitial sites in bcc Fe. The GB region is represented by three layers of interface sites indicated by blue spheres in Fig. 6. Additionally, the three layers above and below the interface region are marked as intermediate sites (red spheres). The structure is highly anisotropic, and diffusion within the interface layers and perpendicular to them is expected to differ significantly. Within the kMC simulations cells with side lengths of $x = y = 11.328$ Å and $z = n \times 11.328$ Å (with $n = 1$–5) are used, which are periodically repeated in all three dimensions.

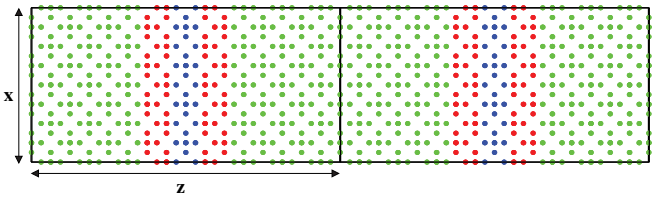

FIG. 6. (Color online) Model of an idealized layered structure of parallel grain boundary regions in bcc Fe. The spheres represent tetrahedral interstitial sites in bcc Fe, each having four nearest neighbors at the same distance. Interface sites, intermediate sites, and bulk sites are shown in blue, red, and green, respectively.

In a first step we investigate the diffusivity of H as a function of the interface-interface distance. Here, the intermediate sites are equivalent to bulk sites; the corresponding barriers are taken from case (I) in Table II. The results of the kMC simulations at $T = 600$ K are shown in Fig. 7. In Figs. 7(a) and 7(b) the diagonal components of the diffusion tensor parallel, $D_{\parallel} = 1/2(D_{xx} + D_{yy})$, and perpendicular, $D_{\perp} = D_{zz}$, to the interface layers are depicted, respectively. Diffusion perpendicular to the interface layers is much slower than parallel to the interface, but in both directions the diffusivity exhibits a linear dependence on the distance between the interface layers. This is due to the probability of finding H atoms within the bulk region, p_{bulk}. According to Eq. (19) at low H concentration (with $\Xi_{\text{bulk}} \approx \Xi_{\text{intf}} \approx 1$) the overall diffusion constant depends linearly on p_{bulk} (with $p_{\text{intf}} = 1 - p_{\text{bulk}}$) where the slope depends on the difference in diffusivity in the bulk and interface regions. Since the diffusivity in the bulk region is higher than in the interface region, the overall diffusivity increases linearly with increasing p_{bulk}. p_{bulk} again increases likewise linearly with increasing interface-interface distance as shown in Fig. 7(c). Since within our current model the condition $\exp(\Delta E_{\text{bind}}/k_{\text{B}}T)(n_{\text{intf}}/n_{\text{bulk}}) \gg 1$ holds (i.e., there is a notable number of interface sites with a significant binding energy), Eq. (24) can further be simplified

$$p_{\text{bulk}} = \frac{n_{\text{bulk}}}{n_{\text{intf}}} \exp\left(\frac{-\Delta E_{\text{bind}}}{k_{\text{B}}T}\right), \tag{26}$$

suggesting that p_{bulk} is proportional to the ratio of bulk and interface sites, $n_{\text{bulk}}/n_{\text{intf}}$, at a given temperature T. As n_{bulk} increases linearly with the interface-interface distance, whereas n_{intf} remains constant, their ratio increases linearly and so does p_{bulk}.

TABLE II. Diffusion barriers, ΔE_i, between various sites i within the idealized layered structure. The three cases represent three different models to approximate different GBs in bcc Fe.

Process i	Case (I)	Case (II)	Case (III)
bulk → bulk	0.088	0.088	0.088
bulk → intermediate	0.088	0.088	0.088
intermediate → bulk	0.088	0.288	0.088
intermediate → intermediate	0.088	0.200	0.088
intermediate → interface	0.088	0.088	0.088
interface → intermediate	0.600	0.400	0.500
interface → interface	0.250	0.550	0.550

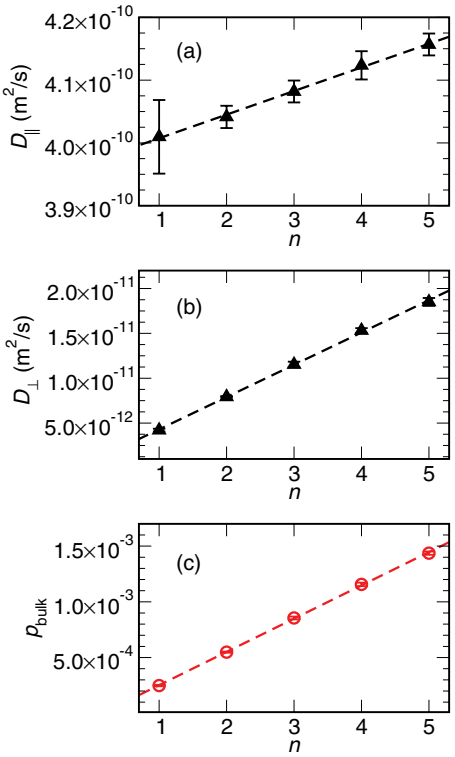

FIG. 7. (Color online) H diffusivity and H distribution as a function of the interface-interface distances within the layered structure: (a) components of the diffusion tensor parallel to the interface, $D_{\parallel} = 1/2(D_{xx} + D_{yy})$; (b) component of the diffusion tensor perpendicular to the interface, $D_{\perp} = D_{zz}$; (c) probability of finding H in the bulk region, p_{bulk}. Symbols denote results from the kMC simulations, and dashed lines correspond to linear fits.

Diffusion perpendicular to the interface layers can be described in an even simpler model. Since the interface region provides traps for H atoms with an energy gain of 0.512 eV and H diffuses rapidly within the bulk region, the diffusion perpendicular to the interface can be approximated by H hopping between two adjacent grain boundary planes. Within this 1D model the hoping rate is $k_{\perp} = \nu_{\perp} e^{-\Delta E_{\perp}/k_{\text{B}}T}$, and

$$D_{\perp} = \Gamma_{\perp} a_{\perp}^2 \nu_{\perp} \exp\left(\frac{-\Delta E_{\perp}}{k_{\text{B}}T}\right). \tag{27}$$

Here, $\Gamma_{\perp} = 2/2 = 1$ and $a_{\perp}$ is the interlayer distance. As discussed, the probability of finding H in the bulk region, p_{bulk}, is proportional to the interlayer distance and thus is the time, τ, that H spends in the bulk region, yielding the relation $p_{\text{bulk}} \sim a_{\perp} \sim \tau = \frac{1}{\nu_{\perp}}$. Hence, the attempt frequency $\nu_{\perp}$ is inversely proportional to $a_{\perp}$, and as a result, the diffusion constant $D_{\perp}$ is proportional to $a_{\perp}$, which is consistent with the results shown in Fig. 7(b). The linear dependence of $1/\nu_{\perp}$ on the interlayer distance is strictly only valid if the bulk region is much thicker than the interface region. With increasing interface-interface distance and in the limit of an infinitely thin interface layer, the effective hopping barrier $\Delta E_{\perp}$ converges to the barrier for escaping from the interface region $\Delta E_{\text{intf}\to\text{bulk}}$.

As a second step the dependence of the diffusivity within the layered structure on the H concentration is investigated. The results of the kMC simulations are shown in Fig. 8 for

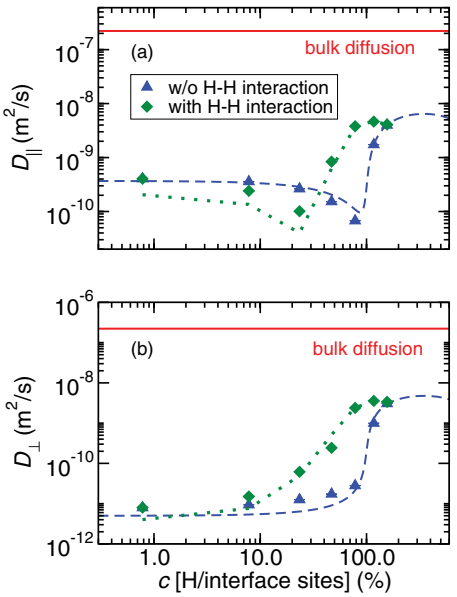

FIG. 8. (Color online) Diffusion constants as a function of H concentration at $T = 600$ K in an idealized layered structure. The diffusivities parallel ($D_{\parallel}$) and perpendicular ($D_{\perp}$) to the interface layers are shown in (a) and (b), respectively. The blue triangles denote the numerical results from the kMC simulations without H-H interactions; the dashed lines are the analytic results obtained via Eq. (19). The green diamonds show the results for kMC simulations including H-H pair interactions; the dotted green lines are obtained from the modified analytic expression (see Appendix). The red curve represents the diffusivity of H in perfect bcc Fe within the dilute limit.

$T = 600$ K. The simulation cell with $z = 22.656$ Å contains 128 interface sites and 1408 bulk sites.

Figure 8(a) illustrates the diffusivity parallel to the interface ($D_{\parallel}$). Similar to the results for the cubic grain structure the diffusivity is constant and lower than bulk diffusion for low H concentrations. When the number of H atoms approaches the number of available interface sites, blocking occurs and a dip is observed for $D_{\parallel}$. For even higher concentrations the diffusivity increases quickly due to contributions from bulk diffusion. The dashed line shows the results of our analytic model obtained from Eq. (19). The fitted geometric prefactors are $\Gamma_{\parallel,\mathrm{intf}} = 0.455$ and $\Gamma_{\parallel,\mathrm{bulk}} = 0.638$, and the numeric and analytic results are in very good agreement. Since the interface layers can be considered as parallel, 2-dimensional planes, the theoretical value for the geometric prefactor is $\Gamma_{\parallel,\mathrm{intf}} = \frac{2}{4} = 0.5$. Within the bulk region the geometric arrangement is unchanged, i.e., $\Gamma_{\parallel,\mathrm{bulk}} = \frac{4}{6} = 0.667$. Again the fitted geometric prefactors are close to the ideal theoretical values.

Figure 8(b) shows the diffusivity perpendicular to the interface plane, $D_{\perp}$, as a function of H concentration. For low concentrations diffusion perpendicular to the interfaces is much slower than parallel diffusion. This is due to the fact that the H atoms are largely confined within the interface region. At large H concentrations bulk diffusion dominates and the diffusivity becomes isotropic. Since diffusion within the interface layers does not significantly contribute to $D_{\perp}$, there is also no blocking effect observed. Instead, the diffusivity increases smoothly as the number of H atoms approaches the number of interface sites and bulk diffusion becomes dominant. The dashed line is obtained within our analytic model. Here, the agreement between numerical and analytic results is also remarkable. The fitted geometric prefactors are $\Gamma_{\perp,\mathrm{intf}} = 0.0$ and $\Gamma_{\perp,\mathrm{bulk}} = 0.470$. The zero value of $\Gamma_{\perp,\mathrm{intf}}$ confirms that diffusion within the interface layers does not contribute to $D_{\perp}$. The value of $\Gamma_{\perp,\mathrm{bulk}}$ is smaller than the expected value of 0.667. The deviation can be explained by the fact that H diffusion in the bulk region perpendicular to the interfaces is interrupted by trapping within the interface planes effectively lowering the overall diffusion constant. It also indicates that our assumption within our analytic model, that the overall diffusion is a weighted sum over the diffusion within the different regions, does not fully apply to $D_{\perp}$. Here, the overall diffusion is a combination of diffusion within the bulk region and trapping within the interface region.

If we include H-H interaction in our kMC model for the layered structure, we observe a change in the diffusivity as compared to neglecting H-H interactions as shown by the green diamonds in Fig. 8. Similar to the results obtained for the idealized cubic model, the overall shape of the curves remains the same. Again the dip in diffusivity for diffusion parallel to the interface occurs at lower H concentrations indicating an effective blocking due to the repulsive H-H interactions. Correspondingly, diffusivity perpendicular to the interface increases at lower H concentrations since the repulsive H-H interactions make it more favorable for H atoms to escape from the interface region at lower concentrations. The dotted green lines in Fig. 8 represent the results of our modified analytic expression as discussed in the Appendix. Again we observe that the agreement is reasonable albeit not as good as for the case without H-H interactions.

In a third step we investigate the influence of different types of GBs on the diffusivity. Our DFT calculations for the $\Sigma 5$ GB in bcc Fe[15] indicate that diffusion perpendicular to the GB interface proceeds via an intermediate site. Furthermore, the more close-packed $\Sigma 3[1\bar{1}0](112)$ GB ($\Sigma 3$ in short) in bcc Fe exhibits rather large diffusion barriers within the interface region as well as perpendicular to it.[15] We consider three different cases for which the barriers are summarized in Table II. Case (I) resembles our original setup where the intermediate and bulk sites are equivalent and the diffusion barrier between interface sites is larger than in the bulk region but still considerably lower than the diffusion barrier out of the interface region. In case (II) intermediate sites are introduced where the diffusion barrier between intermediate sites is lower but almost comparable to the escape barrier into the bulk region. Case (III) resembles the situation within the $\Sigma 3$ GB in bcc Fe. Both the diffusion barrier within and the one perpendicular to the interface region are rather large. As already discussed, for a temperature of $T = 600$ K and in the dilute limit for case (I) hydrogen is largely confined to the interface region and almost the entire diffusion takes place in the interface region, although the diffusion barrier is higher than in the bulk region. In case (II) approximately half of all diffusion processes are found in the intermediate region, which only provides about 1/5 of the available sites. This indicates that diffusion within the intermediate region is preferred, guiding hydrogen along the grain boundary, thereby

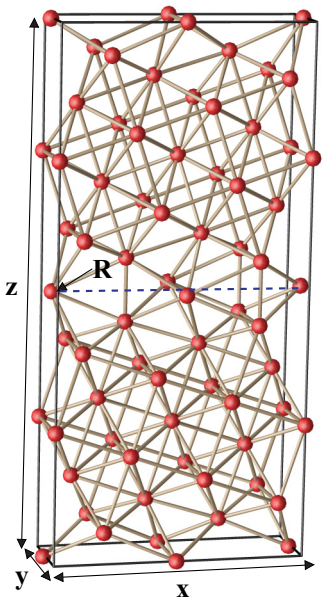

FIG. 9. (Color online) Simulation cell of the Σ5 grain boundary in bcc Fe. The red spheres represent Fe atoms, and the GB interface is indicated by the blue dashed line. All interstitial sites are characterized with respect to a reference atom denoted by R.

partially alleviating the trapping effect of the energetically low lying interface sites. For case (III) we find that the interface region only acts as a trap for hydrogen. Diffusion is almost entirely observed in the bulk region and there is no enhanced diffusivity in the intermediate region, i.e., in this case the GB does not influence the preferred diffusion direction of hydrogen.

Our findings for the idealized layered structures indicate that depending on the nature of the actual GB the interface region might either determine the preferred diffusion direction or trap and effectively immobilize hydrogen atoms at the interfaces. In the next section we extend our layered model to more closely resemble the structure of the Σ5 GB in bcc Fe.

VI. Σ5 GRAIN BOUNDARY IN bcc Fe

The structure of the Σ5 grain boundary in bcc Fe is illustrated in Fig. 9. To set up a kMC model that describes the diffusion of hydrogen within the Σ5 GB, it is necessary to identify all stable interstitial sites for H atoms within this structure as well as possible diffusion processes between these sites. Here we performed extensive DFT calculations to obtain reliable values for solution energies and diffusion barriers. Our results are thus not dependent on any fitted parameters but all input data are extracted from *ab initio* calculations. We have investigated the stability of hydrogen within various interstitial sites in a previous study[15] and found that within the Σ5 GB interstitial sites close to the interface region are energetically more favorable for H atoms than the tetrahedral site in bulk bcc Fe. The DFT calculations revealed 8 distinctive interstitial sites within the Σ5 GB. The relative solution energies of H within these sites with respect to the most stable site (if3) are summarized in Table III.

TABLE III. Relative positions of various symmetry-inequivalent interstitial sites within the Σ5 grain boundary in bcc Fe. The positions are given with respect to the reference atom R in Fig. 9. Solution energies are listed relative to the most stable interstitial site, if3. The relative solution energy of a tetrahedral bulk site is 0.500 eV.

Site	Δx (Å)	Δy (Å)	Δz (Å)	ΔE (eV)
if1	7.041	0.000	0.001	0.050
if2	3.917	0.000	0.007	0.269
if3	5.522	0.000	0.075	0.000
im1	4.249	0.000	0.659	0.237
im2	1.287	0.000	0.759	0.208
im3	7.591	0.000	1.204	0.315
im4	6.854	−0.001	1.504	0.373

To identify suitable transition states for diffusion processes between the various interstitial sites we employed the nudged elastic band method[28,29] as implemented in the VASP code.[30,31] The computational details can be found in Ref. 15. We found 12 different diffusion processes; the corresponding barriers extracted from the DFT calculations are summarized in Table IV.

Based on our very detailed DFT study the kMC model of the Σ5 GB structure is constructed by mapping the 8 identified interstitial sites onto a lattice connected by the 12 diffusion processes listed in Table IV. The $(1 \times 1 \times 1)$ supercell of the Σ5 GB shown in Fig. 9 has the dimensions $x = 8.98$ Å, $y = 2.84$ Å, and $z = 71.78$ Å. In addition to the tetrahedral interstitial sites in the bulk region, the relative positions of the different interstitial sites close to the interface region with respect to a reference atom R (see Fig. 9) are listed in Table III. The reference atom R sits within the GB plane. Due to the mirror symmetry of the GB interface, for an interstitial site at $(\Delta x, \Delta y, \Delta z)$ with $\Delta z > 0.1$ Å, there is an equivalent site at $(\Delta x, \Delta y, -\Delta z)$. Since the Σ5 GB has a base-centered orthorhombic structure, for an interstitial site at $(\Delta x, \Delta y, \Delta z)$ there exists an equivalent site at $(\Delta x + x/2, \Delta y + y/2, \Delta z)$. For the kMC simulations we used a model corresponding to a

TABLE IV. Hydrogen diffusion barriers for possible transitions between interstitial sites in the Σ5 grain boundary in bcc Fe. Values are given for both the forward and backward process. The process im3 ↔ im2 takes place between second-nearest neighbors, while all other transitions are between nearest-neighbor sites.

Process	$\Delta E_{\text{forward}}$ (eV)	$\Delta E_{\text{backward}}$ (eV)
if3 ↔ if1	0.118	0.068
if1 ↔ im3	0.339	0.074
im3 ↔ im2	0.109	0.216
im2 ↔ bulk	0.383	0.091
if3 ↔ im4	0.429	0.056
if2 ↔ im1	0.020	0.052
im1 ↔ if3	0.102	0.339
im4 ↔ bulk	0.201	0.074
bulk ↔ bulk	0.088	0.088
if3 ↔ if3	0.250	0.250
if3 ↔ im2	0.241	0.033
im4 ↔ im3	0.030	0.088

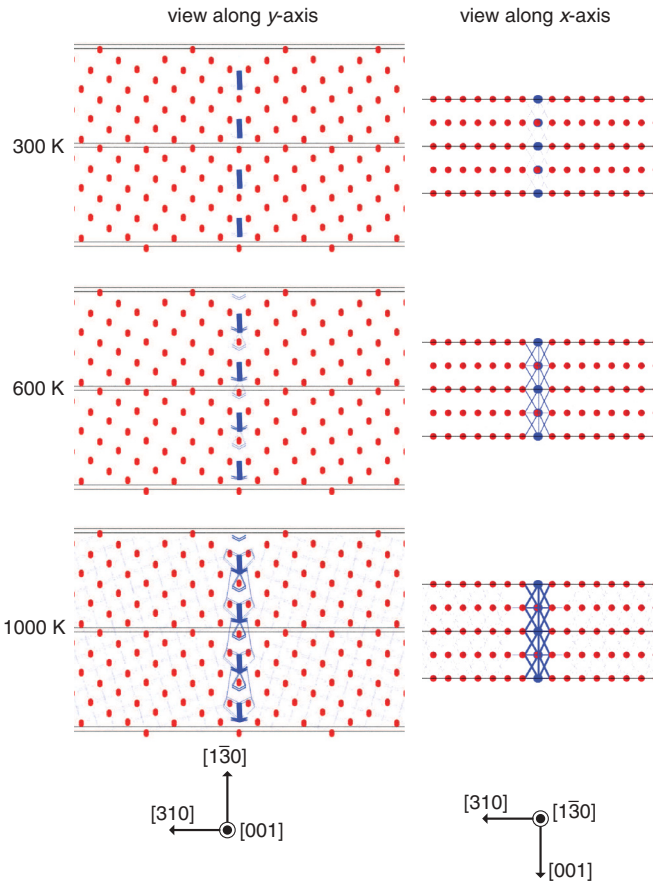

FIG. 10. (Color online) Diffusion network within the Σ5 GB. The red spheres represent Fe atoms, and the blue lines illustrate the diffusion probabilities for various H diffusion paths.

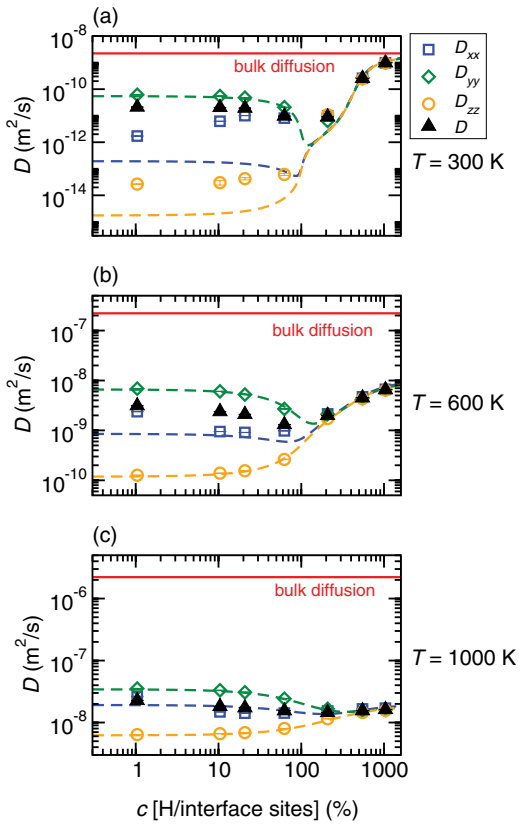

FIG. 11. (Color online) Components of the diffusion constant tensor as a function of H concentration within the Σ5 GB in bcc Fe. Results are shown for (a) 300 K, (b) 600 K, and (c) 1000 K. The kMC results for D_{xx}, D_{yy}, D_{zz}, and the overall diffusivity D are represented by blue squares, green diamonds, orange circles, and black triangles, respectively. The analytic results are shown as dashed lines in the corresponding color. The red curve represents the diffusivity of H in perfect bcc Fe within the dilute limit.

$(2 \times 6 \times 1)$ supercell that is repeated periodically in all three dimensions. The model contains 48 if1, 48 if2, 48 if3, 96 im1, 96 im2, 96 im3, 96 im4, and 10 224 bulk sites.

The interstitial sites and microscopic diffusion processes create a complex diffusion network for hydrogen that is highly anisotropic. To illustrate this network the contribution of different processes to the overall diffusivity is shown in Fig. 10 for low H concentrations. The relative line thickness corresponds to the relative probabilities of observing H atoms diffuse along this connection. For all three temperatures of $T = 300$, 600, and 1000 K, diffusion within the bulk region is negligible. Thus, diffusion in the z direction is slow since for this hydrogen has to leave the interface region and cross the bulk region towards the next interface. The plots on the left side of Fig. 10 show a view along the y axis, [001] direction, illustrating the diffusion network in the x direction. Although there is a thick connection between the if3 and if1 site there exists no continuous diffusion pathway within the interface. To diffuse in the x direction hydrogen has to leave the interface taking less favorable paths. Thus diffusivity in the x direction is low for small hydrogen concentrations as also shown in Fig. 11. For the diffusion in the y direction hydrogen can continuously move along if3 sites without leaving the interface region as shown in the plots on the right side of Fig. 10 (view along the x axis, [1$\bar{3}$0] direction). With increasing temperature the diffusion network becomes more isotropic within the interface plane. This is also reflected in the different components of the diffusion tensor shown in Fig. 11. For $T = 300$ K at low H concentrations D_{xx} and D_{yy} differ by almost two orders of magnitude, whereas at $T = 1000$ K they are comparable.

As discussed in the previous sections, for the idealized interface structures the diffusivity shows a strong dependence on the hydrogen concentration. In Fig. 11 the diagonal components of the diffusion constant tensor as a function of the hydrogen concentration are shown for $T = 300$, 600, and 1000 K for the Σ5 GB. For low H concentrations diffusion in the interface region dominates and the diffusivity is anisotropic as expected from the discussion of the diffusion network. For large H concentrations diffusion is again isotropic since bulk diffusion dominates. The overall diffusion constants measured in the kMC simulations are the result of the statistical interplay of all possible diffusion processes. In our simple analytic model diffusion within a certain site type is associated with one specific barrier, whereas in the Σ5 GB there are several processes and thus barriers associated with one site type and diffusion within the interface layer proceeds via several site types. It is thus not possible to accurately describe the diffusivity within our simple analytic model in Eq. (19).

Nevertheless, in order to obtain an understanding of how much the diffusions within the GB interface and the bulk region contribute to the diffusion constant, we approximate the diffusivity within Σ5 GB by selected and/or combined processes within the analytic model.

H diffusion along the x direction and within the GB interface follows the path if3 → im4 → im3→ im2 → if3 (see Fig. 10). We assume that this diffusion path is dominated by the step if3 → im4 with a barrier of 0.429 eV. Following Eq. (19), we approximate the diffusivity in the x direction, D_{xx}, as

$$D_{xx} = p_{\mathrm{if3}}(T) D_{0,xx,\mathrm{if3}} \exp\left(\frac{-\Delta E_{\mathrm{if3}\to\mathrm{im4}}}{k_{\mathrm{B}}T}\right) \Xi_{\mathrm{if3}}(T, N_{\mathrm{H}}) + p_{\mathrm{bulk}}(T) D_{0,xx,\mathrm{bulk}} \exp\left(\frac{-\Delta E_{\mathrm{bulk}}}{k_{\mathrm{B}}T}\right) \Xi_{\mathrm{bulk}}(T, N_{\mathrm{H}}), \tag{28}$$

with $D_{0,xx,s} = \Gamma_{xx,s} a_{xx,s}^2 \nu_0$. The other contributions to the sum are neglected. Still, as in the case of isolated point defects, the other interstitial sites influence the hydrogen distribution and thus the corresponding probabilities in Eq. (28). The hop length between two adjacent if3 sites along the x direction is $a_{xx,\mathrm{if3}} = 4.486$ Å.

Along the y direction, the overall diffusion constant, D_{yy}, is similarly approximated within our analytical model. Diffusion in the y direction either takes place within the bulk region or in between if3 sites. For the hop between two adjacent if3 sites along the y direction, the hop length is $a_{yy,\mathrm{if3}} = 2.837$ Å and the barrier $\Delta E_{\mathrm{if3}\to\mathrm{if3}} = 0.250$ eV; the other diffusion processes are not taken into account.

As discussed in Sec. V, for H diffusion along the z direction (perpendicular to the interface), the GB interface acts like a point trap. All geometric prefactors for diffusion between interface sites are essentially zero, and only bulk diffusion contributes to D_{zz}.

The analytic results are shown together with the kMC results in Fig. 11. For D_{yy} the agreement is excellent, indicating that diffusion in bulk and along if3 sites are indeed the dominating processes. For D_{xx} and D_{zz} the analytic results deviate from the numeric data, especially for lower temperatures. Still, considering the simplicity of our analytic model the agreement is quite remarkable for $T = 600$ and 1000 K.

The fitted values of the geometric prefactors are in the x direction $\Gamma_{xx,\mathrm{if3}} = 1.531$, $\Gamma_{xx,\mathrm{bulk}} = 0.747$; in the y direction $\Gamma_{yy,\mathrm{if3}} = 1.074$, $\Gamma_{yy,\mathrm{bulk}} = 0.701$; and in the z direction $\Gamma_{zz,\mathrm{bulk}} = 0.705$. All bulk values are relatively close to the theoretical value of 0.667. Diffusion in the y direction along if3 sites corresponds essentially to a 1D chain with two nearest neighbors, yielding a theoretical value of $\Gamma_{yy,\mathrm{if3}} = 2/2 = 1$. The good agreement between fitted and theoretical values for the geometric prefactors in the y direction also indicates that the simple analytic model is suitable here.

Diffusion within the y direction, D_{yy}, exhibits a small blocking effect as seen within our idealized models, which is again most pronounced for low temperatures and vanishes at higher temperatures. At $T = 1000$ K there is no dip, but D_{yy} somewhat decreases with increasing H concentration. This is due to the fact that at 1000 K the effective diffusion constant within the bulk region is actually smaller than in between interface sites; i.e., $D_{yy,\mathrm{bulk}} < D_{yy,\mathrm{if3}}$ with $D_{yy} = p_{\mathrm{if3}} D_{yy,\mathrm{if3}} \Xi_{\mathrm{if3}} + p_{\mathrm{bulk}} D_{yy,\mathrm{bulk}} \Xi_{\mathrm{bulk}}$ [see Eq. (28)]. The diffusion barrier between if3 sites is larger than between bulk sites, but at high temperatures the prefactor, which is about a factor of 10 larger for diffusion between if3 sites, dominates. Thus at high concentrations where bulk diffusion has the largest contribution the overall diffusivity, D_{yy}, decreases. At all temperatures, diffusion perpendicular to the interface planes, D_{zz}, is slowest, due to trapping of H within the grain boundary region. With respect to diffusion in the x direction (D_{xx}) the kMC results for $T = 300$ K suggest that the if3 site likewise acts as a point trap. At this low temperature H atoms that occupy if3 sites are nearly immobile in the x direction. Once the H concentration reaches that of if3 sites, diffusion in the x direction may occur following the path im2 ↔ bulk → im2 or im4 → bulk → im4 with smaller diffusion barriers of 0.38 eV and 0.21 eV, respectively. These effectively lower barriers are also consistent with the increase and relatively large value of D_{xx} with increasing H concentration as shown in Fig. 11(a). For high temperatures and high H concentrations bulk diffusion dominates and the diagonal components of the diffusion tensor are equivalent, indicating an isotropic diffusion behavior. In all cases the overall diffusion in the grain boundary structure is slower than diffusion in perfect bcc Fe bulk.

It is apparent that for the more realistic model of the Σ5 GB in bcc Fe our analytic model is too simple to fully describe the diffusion of hydrogen. Nevertheless, the observed trends at high temperatures may be understood qualitatively with a simple analytic approximation. Based on the kMC results, a diffusion network was established and the processes that dominate the diffusion under various conditions were extracted yielding a more detailed understanding of hydrogen diffusion within grain boundary structures.

VII. CONCLUSIONS

Employing kinetic Monte Carlo simulations we have studied hydrogen diffusion within various models representing different arrangements of grain boundaries and point defects in bcc Fe. The defect regions exhibit interstitial sites with a significantly lower solution energy for H atoms, effectively acting as trapping sites. Within an idealized cubic grain structure we observe a characteristic behavior of the diffusion tensor as a function of hydrogen concentration. At low concentrations H is confined to the interface region and the diffusivity is low as compared to diffusion in perfect bcc Fe bulk. As the number of H atoms approaches the number of interface sites the diffusion constant drops due to blocking of available interstitial sites. At large H concentrations bulk diffusion dominates the behavior and a significant increase of the diffusivity is observed. Taking into account H-H interactions within the idealized cubic grain we observe that the overall dependence of the diffusivity on the H concentration is maintained, but the dip in diffusivity occurs at much lower H concentrations. This is due to an effective blocking resulting from the repulsive H-H interactions. Large concentrations of additional point defects lower the diffusivity for small H concentrations, but do not change the behavior for larger concentrations. Also, at realistic defect concentrations the effect appears to be negligible.

Within a layered arrangement of grain boundary planes the diffusion is anisotropic. Parallel to the interface diffusion is similar to the one observed within the grain structure. Perpendicular to the interface diffusion is much slower and can effectively be described by a 1D model of H atoms hopping between neighboring interface planes. The effect of the grain boundary on the diffusion of hydrogen strongly depends on the actual solution energies and diffusion barriers between different interstitial sites. The effect of H-H interactions in the layered structure is similar to the idealized cubic grain: The overall dependence of the diffusivity on H concentration remains the same, but a shift to lower H concentrations is observed.

The more detailed model of the $\Sigma 5$ GB in bcc Fe showed that the overall diffusion is a complex interplay of various microscopic diffusion processes. Depending on the conditions (hydrogen concentration, temperature, diffusion direction) different processes dominate the diffusion resulting in a complex diffusion network. Still, the general trends with respect to temperatures and hydrogen concentrations may be understood from a simplified analytic model.

We have derived a simple, analytical expression for hydrogen diffusion within microstructures that consist of several distinctive regions (such as bulk, interfaces, point defects). The analytic model is in very good agreement with the numerical results for the idealized structures. Including H-H interactions imposes, however, a configuration dependence of the solution energies and diffusion barriers which makes it impossible to derive a simple analytic expression and requires more sophisticated approaches. Likewise, for the more detailed model of the $\Sigma 5$ GB the analytic model only works for conditions where the diffusion is dominated by a few, specific processes, but naturally it fails to capture the more complex interplay between a number of different microscopic diffusion processes.

In all structures the diffusivity is lower than in perfect bcc Fe bulk, indicating that the grain boundary regions do not serve as fast diffusion channels. Nevertheless, at low concentrations hydrogen is confined to the interface region; i.e., the arrangement of grain boundary planes and thus the microstructure significantly influences the preferred diffusion direction.

ACKNOWLEDGMENTS

The authors acknowledge financial support through ThyssenKrupp AG, Bayer MaterialScience AG, Salzgitter Mannesmann Forschung GmbH, Robert Bosch GmbH, Benteler Stahl/Rohr GmbH, Bayer Technology Services GmbH, and the state of North-Rhine Westphalia, as well as the EU in the framework of the ERDF.

APPENDIX: INCLUDING H-H INTERACTIONS IN THE ANALYTIC MODEL

The H-H interactions introduce a concentration dependence of the solution energies and diffusion barriers. It is thus not possible to derive the probability of finding H in a certain site type, p_s, from Eq. (11). To obtain an estimate of the diffusivity from our analytic model in Eq. (19), we have used the numerical results for p_s as obtained from the corresponding kMC simulations. In addition, the repulsive H-H interactions can be viewed to a first approximation as an additional factor that effectively enhances the blocking effect. We thus modify the blocking in Eq. (20) as

$$\Xi_s(T,N_{\mathrm{H}}) = \left(1 - C \times \frac{\overline{N}_{\mathrm{H},s}(T,N_{\mathrm{H}})}{n_s}\right). \tag{A1}$$

The constant C reflects the enhanced blocking and is fitted to the numerical results. Only one value of C is used for all site types. Within the idealized cubic grains a value of $C = 3.55$ is obtained. Since each hydrogen atom has at most two second-nearest neighbors in a lattice of tetrahedral sites in bcc, a maximum fractional occupancy of $f_{\max} = 0.25$ is expected. This is close to the fitted value of $1/C = 0.28$. Using the modified blocking factor and the numerical values for the probabilities p_s the dotted lines in Fig. 3 are obtained.

The same approach is used to estimate analytic results for the idealized layered structure (dotted lines in Fig. 8). For diffusion parallel to the interface a value of $C_{\parallel} = 5.21$ is obtained. The much higher value of $C_{\parallel}$ is due to the quasi-two-dimensional diffusion within the interface region and thus an effectively lower fractional occupancy. For diffusion perpendicular to the interface a value of $C_{\perp} = 3.10$ is obtained. The magnitude of the constant C indicates hereby the strength of the repulsive interactions.

Since the blocking factor cannot become negative, the approximation is restricted to hydrogen concentrations that do not exceed the maximum fractional occupancy $1/C$ within each site type.

*jutta.rogal@rub.de

[1] P. Novak, R. Yuan, B. Somerday, P. Sofronis, and R. Ritchie, J. Mech. Phys. Solids **58**, 206 (2010).
[2] A. Ramasubramaniam, M. Itakura, M. Ortiz, and E. Carter, J. Mater. Res. **23**, 2757 (2008).
[3] M. Wen, S. Fukuyama, and K. Yokogawa, Acta Mater. **51**, 1767 (2003).
[4] L. Zhong, R. Wu, A. J. Freeman, and G. B. Olson, Phys. Rev. B **62**, 13938 (2000).
[5] J. P. Hirth, Metall. Mater. Trans. A **11**, 861 (1980).
[6] C. D. Beachem, Metall. Trans. **3**, 437 (1972).
[7] H. K. Birnbaum, Mater. Sci. Eng. A **176**, 191 (1994).
[8] J. von Pezold, L. Lymperakis, and J. Neugebauer, Acta Mater. **59**, 2969 (2011).
[9] R. A. Oriani and P. H. Josephic, Acta Metall. **22**, 1065 (1974).
[10] R. A. Oriani and P. H. Josephic, Acta Metall. **25**, 979 (1977).
[11] R. A. Oriani, Annu. Rev. Mater. Sci. **8**, 327 (1978).
[12] S. Lee and D. Unger, Eng. Fract. Mech. **31**, 647 (1988).
[13] W. W. Gerberich, T. Livne, X. F. Chen, and M. Kaczorowski, Metall. Mater. Trans. A **19**, 1319 (1988).
[14] R. Nazarov, T. Hickel, and J. Neugebauer, Phys. Rev. B **82**, 224104 (2010).

[15] Y. A. Du, L. Ismer, J. Rogal, T. Hickel, J. Neugebauer, and R. Drautz, Phys. Rev. B **84**, 144121 (2011).
[16] P. Hohenberg and W. Kohn, Phys. Rev. B **136**, 864 (1964).
[17] W. Kohn and L. J. Sham, Phys. Rev. A **140**, 1133 (1965).
[18] D. E. Jiang and E. A. Carter, Phys. Rev. B **70**, 064102 (2004).
[19] Y. Fukai and H. Sugimoto, Advances in Physics **34**, 263 (1985).
[20] M. Nagano, Y. Hayashi, N. Ohtani, M. Isshiki, and K. Igaki, Scr. Metall. **16**, 973 (1982), and references therein.
[21] Z. Qi, J. Volkl, R. Lasser, and H. Wenzl, J. Phys. F **13**, 2053 (1983).
[22] V. Lottner, J. Haus, A. Heim, and K. Kehr, J. Phys. Chem. Solids **40**, 557 (1979).
[23] V. Lottner, A. Heim, and T. Springer, Z. Phys. B **32**, 157 (1979).
[24] R. Kirchheim, Prog. Mater. Sci. **32**, 261 (1988).
[25] A. B. Bortz, M. H. Kalos, and J. L. Lebowitz, J. Comp. Phys. **17**, 10 (1975).
[26] D. T. Gillespie, J. Comp. Phys. **22**, 403 (1976).
[27] G. H. Vineyard, J. Phys. Chem. Solids **3**, 121 (1957).
[28] H. Jónsson, G. Mills, and K. W. Jacobsen, in *Classical and Quantum Dynamics in Condensed Phase Simulations*, edited by B. J. Berne, G. Ciccotti, and D. F. Coker (World Scientific, Singapore, 1998), pp. 385–404.
[29] G. Henkelman and H. Jónsson, J. Chem. Phys. **113**, 9978 (2000).
[30] G. Kresse and J. Hafner, Phys. Rev. B **47**, 558(R) (1993).
[31] G. Kresse and J. Furthmüller, Phys. Rev. B **54**, 11169 (1996).
[32] J. P. Perdew, J. Chevary, S. Vosko, K. A. Jackson, M. R. Pederson, D. J. Singh, and C. Fiolhais, Phys. Rev. B **46**, 6671 (1992).
[33] J. P. Perdew, J. Chevary, S. Vosko, K. A. Jackson, M. R. Pederson, D. J. Singh, and C. Fiolhais, Phys. Rev. B **48**, 4978 (1993).
[34] K. A. Fichthorn and W. H. Weinberg, J. Chem. Phys. **95**, 1090 (1991).
[35] R. Kirchheim, Acta Metall. **35**, 271 (1987).
[36] A. Allnatt and A. Lidiard, *Atomic Transport in Solids* (Cambridge University Press, Cambridge, 1993).
[37] The calculations were performed using the generalized gradient approximation (GGA, PW91) for the exchange correlation functional, an energy cutoff for the plane waves of 350 eV, and a [4 × 4 × 4] Monkhorst-Pack grid for the integration of the Brillouin zone.
[38] P. Kratzer, in *Multiscale Simulation Methods in Molecular Sciences*, edited by J. Grotendorst, N. Attig, S. Blügel, and D. Marx, Vol. 42 of NIC series (John von Neumann Institute for Computing/Forschungszentrum Jülich, Germany, 2009), p. 51.
[39] R. Kirchheim and U. Stolz, J. Non-Cryst. Solids **70**, 323 (1985).
[40] Y. Tateyama and T. Ohno, Phys. Rev. B **67**, 174105 (2003).
[41] M. I. Mendelev and Y. Mishin, Phys. Rev. B **80**, 144111 (2009).
[42] R. A. Oriani, Acta Metall. **18**, 147 (1970).